





Original Article


Numerical investigation on the fatigue failure characteristics of water-bearing sandstone under cyclic loading



ZHU Chun^{1,2,4}  <https://orcid.org/0000-0003-2867-6478>; e-mail: zhuchuncumtb@163.com

HE Man-chao²  <https://orcid.org/0000-0002-5430-4021>; e-mail: manchaohecumtb@163.com

JIANG Bei²  <https://orcid.org/0000-0002-3323-5557>; e-mail: jiangbei519@163.com

QIN Xin-zhan^{2,4}  <https://orcid.org/0000-0002-5987-3549>; e-mail: 925917595@qq.com

YIN Qian²  <https://orcid.org/0000-0001-5161-3761>; e-mail: Jeryin@foxmail.com

ZHOU Yu^{3*}  <https://orcid.org/0000-0001-8436-8766>;  e-mail: zhouyu@usx.edu.cn

*Corresponding author

¹ School of Earth Sciences and Engineering, Hohai University, Nanjing 210098, China

² State Key Laboratory for Geomechanics & Deep Underground Engineering, Beijing 100083, China

³ Key Laboratory of Rock Mechanics and Geohazards of Zhejiang Province, Shaoxing University, Shaoxing 312000, China

⁴ School of Civil, Environmental and Mining Engineering, The University of Adelaide, Adelaide 5005, SA, Australia

Citation: Zhu C, He MC, Jiang B, et al. (2021) Numerical investigation on the fatigue failure characteristics of water-bearing sandstone under cyclic loading. *Journal of Mountain Science* 18(12). <https://doi.org/10.1007/s11629-021-6914-0>

© Science Press, Institute of Mountain Hazards and Environment, CAS and Springer-Verlag GmbH Germany, part of Springer Nature 2021

Abstract: The strength of sandstone decreases significantly with higher water content attributing to softening effects. This scenario can pose a severe threat to the stability of reservoirs of pumped storage power stations developed from abandoned mines, especially when subjected to the cyclic loading condition caused by the repeated drainage and storage of water (fatigue damage). Based on this, it is essential to focus on the fatigue failure characteristics. In this study, the mineral composition of the used sandstone of Ruineng coal mine in Shanxi Province, China, was first tested to elucidate the rock softening mechanism after absorbing water. Next, a numerical model for replicating the mechanical behavior of water-bearing sandstone was established using two-dimensional particle flow code (PFC2D) with a novel contact model. Then, 16 uniaxial cyclic loading simulations with distinct loading parameters related

to reservoir conditions (loading frequency, amplitude level, and maximum stress level) and different water contents were conducted. The numerical results show that all these three loading parameters affect the failure characteristics of sandstone, including irreversible strain, damage evolution, strain behavior, and fatigue life. The influence degree of these three parameters on failure behavior increases in the order of maximum stress level, loading frequency, and amplitude level. However, for the samples with different water contents, their failure characteristics are similar under the same loading conditions. Furthermore, the failure mode is almost unaffected by the loading parameters, while the water content plays a significant role and causing the transformation from the tensile splitting with low water content to the shear failure with higher water content.

Keywords: Discrete element simulation; Water-bearing sandstone; Cyclic loading parameters; Fatigue failure characteristics; Water content

Received: 26-May-2021

Revised: 10-Sep-2021

Accepted: 24-Sep-2021

1 Introduction

Owing to the urgent need of renewable and clean energy, constructing the pumped storage power stations is one of the feasible methods. To reduce the construction cost, the roadways of the abandoned mines can be used as reservoirs of pumped storage power stations, which exhibit the advantages of large area, significant height differences, and sufficient water source (Tao et al. 2018; Zhu et al. 2019). The rock made up the roadway is usually subjected to physical and chemical effects, decreasing the mechanical properties of rock. For the chemical effect, the chemical dissolution can motivate crack propagation (Li et al. 2020, 2018). Regarding the physical effect, during the operation of pumped storage power stations, the repeated drainage and storage of water is performed as the cyclic loading and unloading conditions to the surrounding rock. Currently, the mechanical properties of water-bearing rock have been extensively studied. For example, two sets of wet and dry shale samples were tested and analyzed by Li et al. (2019), and found that with the increase of water content, the Young's moduli decreases, and the Poisson's ratios increased. The wet specimens also had a slightly stronger anisotropic ratio of elastic moduli compared to dry samples. A theoretical model was built for representing the weakening of rock strength and modulus caused by water absorption in a rock substrate, and mathematical relationships were proposed. The softening of a siltstone sample due to water absorption was simulated based on the theoretical model (Guo et al. 2018).

In rock engineering of reservoirs, the rocks suffer from cyclic loading caused by water. The deformation and failure behavior of rock under cyclic loading tests have been widely studied based on laboratory experiments (Geranmayeh-Vaneghi et al. 2018; Li et al. 2021a, 2021b; Liu et al. 2012; Liu et al. 2018a, 2018b, 2018c; Meng et al. 2018; Peng et al. 2019). The P-wave velocity was found to decrease with the increasing cyclic number, vice the damage rate (Feng et al., 2020a, 2020b). Geranmayeh-Vaneghi et al. (2018) concluded that the failure mode of sandstone under uniaxial cyclic loading conditions is different from the uniaxial compression, which exhibits more local cracks. Liu et al. (2012) found that the axial strain and residual volumetric strain of sandstones increase with confining pressure under cyclic loading,

as did the shear fracture planes. Liu et al. (2018a, 2018b, 2018c) investigated the cyclic loading parameters (i.e., maximum stress, loading amplitude, frequency, duration) on the mechanical behaviors of rock samples, and found that they have no influence on the failure mode which mainly exhibit tensile splitting failure. Based on the thermodynamics theory, an innovative method was introduced by Meng et al. (2018), and the rock energy density under different loading and unloading rates was calculated. Both the fatigue strength and Young's modulus are smaller for the saturated sandstone samples when compared with the dried ones (Bagde et al. 2005; Feng et al. 2019; Niu et al. 2018; Zhao et al. 2018). In addition, they found that the accumulated dissipated energy and acoustic emission energy are also lower, and more macroscopic failure cracks generate.

Next, with the development of computer technology, numerical simulation methods were also used to analyze the failure characteristics of rock (Liu et al. 2021; Qin et al. 2019; Song et al. 2019). Wang et al. (2019) have studied the microdamage regulations of sandstone under cyclic loading conditions with different frequencies and stress levels. A reduction model was embed in the discrete element method by Liu et al. (2017) to simulate the dynamic properties of intermittent jointed rock models during cyclic uniaxial compression, and it revealed that joint geometries control the failure mode. The cracking behavior of sandstone was also found related to the material inhomogeneity (Xiao et al. 2021).

To date, although numerous studies have been conducted on the fatigue failure behavior of sandstone (i.e., dried, and saturated) under cyclic loading conditions, few studies have systematically explored the effect of the water content and cyclic loading parameters related to the storage condition of reservoir. Therefore, the main aim of this study is to analyze the failure characteristics of water-bearing sandstone samples under cyclic loading and unloading using PFC2D software, providing a reference for the construction of reservoirs of pumped storage power stations using the abandoned mines.

2 Mineral Composition Analysis of Test Sample

2.1 Rock sample selection

In the present work, the sandstones in the

roadway floor of Ruineng coal mine in Shanxi Province were selected. The rock samples were prepared based on the ISRM standard with a diameter of 50 mm and a height of 100 mm (± 1 mm).

2.2 Mineral composition analysis

The corresponding composition and content of rock mineral and clay mineral of rock sample were tested by conducting an X-ray diffraction experiment based on the Rigaku TTR-III at the Sinopec Research Institute of Petroleum Processing. The instrument was mainly used for the qualitative and quantitative analysis of crystal structure and phase of mineral.

The results of rock mineral composition and clay mineral of rock samples are shown in Table 1 obtained through X-ray diffraction analysis, indicating that the sandstone samples mainly consists of quartz, plagioclase, and clay minerals. Quartz has characteristics of high hardness, high stability, and strong weathering resistance. The proportion of feldspar is more than 30%, while that of the calcite and dolomite is low. When feldspar is subjected to different degrees of chemical weathering, its hardness is lower than that of quartz, and calcite and dolomite are corrosive. The proportions of clay mineral is around 15.0%, which is the primary factor causing softening of rock after absorbing water (Azhar et al. 2020). The clay mineral mainly comprises of kaolinite, illite, and chlorite, and the proportion of kaolinite is 75%.

Table 1 Mineral analysis of rock samples

Number	Mineral types and proportion (%)					
	Quartz	Plagioclase	Potash feldspar	Calcite	Iron dolomite	Clay
C-10	40.0	18.6	9.0	17.7	4.7	10.0
C-40	33.0	16.5	13.5	21.2	5.0	10.8
C-70	49.3	25.4	6.6	0.3	2.8	15.6
C-100	49.8	24.9	6.4	0.2	0.2	18.5

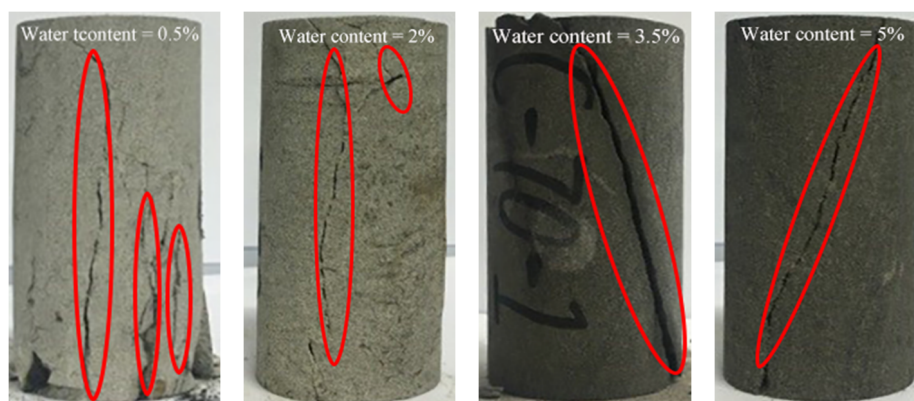


Fig. 1 Typical failure modes of sandstone samples with different water contents under uniaxial compression.

3 Numerical Model Establishment of Water-Bearing Sandstone

3.1 Failure mode of sandstone with different water-contents

To realistically mimic the sandstones in the simulation, their mechanical behaviors are essential. The water absorption tests were first conducted and the results show that the natural water content of the used rock is 0.5%, and the saturated water content of rock is 5%. To study the failure characteristic of rock with different water contents under uniaxial compression test, rocks with four water-contents (0.5%, 2%, 3.5%, and 5%) were selected to carry out the uniaxial compression tests.

By comparing the typical failure characteristics of sandstone after uniaxial compression test (Fig. 1), it was found that the failure mode transfers from tensile splitting failure to single inclined shear failure. The samples with a lower water content have obvious debris falling and block separation during the loading process, and obvious dense small cracks and fissures are formed. With the increase of water content, the number of small cracks and debris decreases. Almost no obvious small crack appears when the samples were saturated, but only a penetrating shear inclined crack. This is because the interaction between clay minerals in sandstone samples becomes worse due to the effect of water, and makes it easier to generate macro fracture.

3.2 Microstructure analysis of sandstone samples with different water contents

The Scanning Electron Microscope (SEM) results of rock samples (Fig. 2) show that the surface of the natural sandstone sample is relatively rough compared with those with higher water contents, which is in accordance with the finding obtained by Feng et al. (2019). With the increase of water content, due to the fact that the particle volume expands and the solution of the minerals like feldspar and clay, the mineral particles show the argillization phenomenon and a large number of flaky structures appear. The grain outline becomes clear, and the number of pores decreases, which leads to the degradation of connectivity. Moreover, as the friction coefficient decreases, the strength of rock further decreases accordingly. Therefore, the macroscopic mechanical properties of rock samples gradually weakened with the increase of water content.

3.3 Model establishment and calibration

Under the complex conditions where the rock is generated, it is impossible to obtain two rock samples with the same properties (e.g., mineral proportion, mineral distribution), while this issue could be well

solved based on numerical simulations. Two-dimensional Particle Flow Code (PFC2D) based on the plain strain hypothesis has been verified by numerous studies that it can be used to investigate the crack evolution in brittle rocks (Ghazvinian et al. 2014; Nguyen et al. 2019; Yang et al. 2019). For PFC2D simulation, a material is modeled as the aggregation of particles. Each particle is in contact with the neighboring particles via the contact model (e.g., linear contact model, parallel-bond contact model, and flat-joint contact model).

In this study, as the water-bearing sandstone is characterized by the softening behavior (with the increase of water content, the strength and stiffness (before and after failure) decrease, shown in Fig. 5(a)), the novel soft-bond contact model (Itasca 2018), for which, it will enter into a softening regime before reaching failure stress, was selected to perform numerical simulations of sandstone. Besides the softening characteristics, its behavior is similar to the widely used linear parallel bond model, with the possibility for the bond to fail if the bond strength is exceeded either in shear or in tension. The softening methodology before failure is based on changing the bond elongation, which controls the softening rate:

$$l^* = l_c(1.0 + \zeta) \tag{1}$$

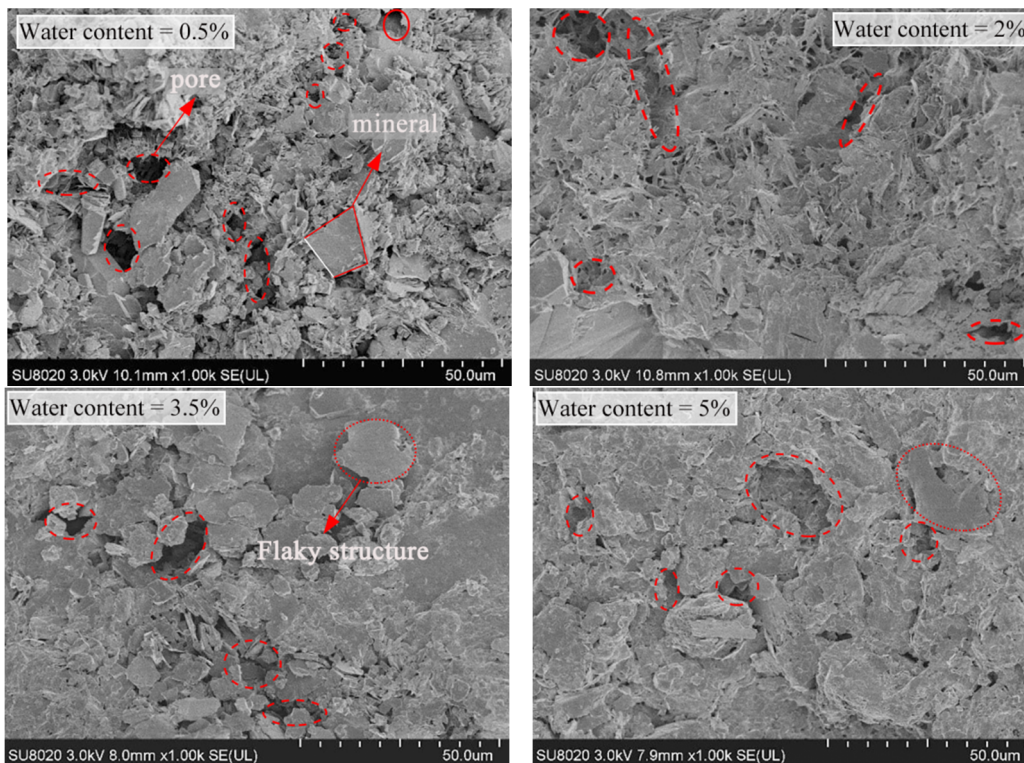


Fig. 2 Scanning electron microscope results of sandstone samples with different water contents.

where l^* is the final bond elongation, l_c is the critical bond elongation and ζ is the softening factor.

After reaching the softening regime, the maximum stress is given by:

$$\sigma^* = \frac{\sigma_c(l^* - l)}{l_c} \tag{2}$$

where l is the current bond elongation, σ_c is the tensile strength. If the current tensile stress is greater than σ_c , the bond contact fails in tension. Otherwise, the shear failure is assessed ($\tau > \tau_c$).

Regarding the strength and stiffness (before failure) degradation attributes to the water, both the effective moduli, cohesion, and tensile strengths are decreased by multiplying a factor of γ , which is suitable to be chosen as the reciprocal of the softening factor after several trials.

The size of the samples is consistent with those in the experiments. The clustered assembly approach was used to generate a randomly distributed grain-based sandstone sample, and the compositions are based on real sandstone. In addition, because the strength of grain boundary is different from the grain, hereafter, rock model contains intragranular (inside one grain) and intergranular (between two grains) contacts. When rock fails, intragranular and intergranular cracks will be generated. The established rock sample models are shown in Fig. 3. In Fig. 3a, the black body is quartz, the gray body is feldspar, and the brown body is clay mineral. In Fig. 3b, the red parts indicate the intragranular contacts, and the black parts indicate the intergranular contacts.

After establishing the sample model, the simulations of the uniaxial compression test were conducted to calibrate the microproperties (i.e., contact properties). The initial calibration was based on the sample with water content of 0.5%. Physical properties of minerals are estimated by numerous mineral identification references (Horn et al. 1962; Morrow et al. 2000): the quartz has the greatest elastic modulus and strength, followed by the feldspar, and then the clay; the Poisson’s ratio is in the subsequent of feldspar, quartz, and clay. During the simulations of uniaxial compression, the loading velocity of upper and bottom walls was set as 0.05 m/s based on the empirical suggestion (Zhang et al. 2014), when the specimen can be regarded to be in a quasi-static state. The details of the calibration procedure are reported in the cited reference (Li et al. 2018). The microparameters obtained after the calibration are shown in Table 2.

To further calibrate the model with different

water contents, the softening factor was used to replicate the weakening phenomenon of rock with the increase of water content. Relevant uniaxial compression test simulations were conducted based on the calibrated model with different softening factors. The distribution characteristics of microcracks of rock samples are shown in Fig. 4a, and the crack number of each sample is shown in Fig. 4b.

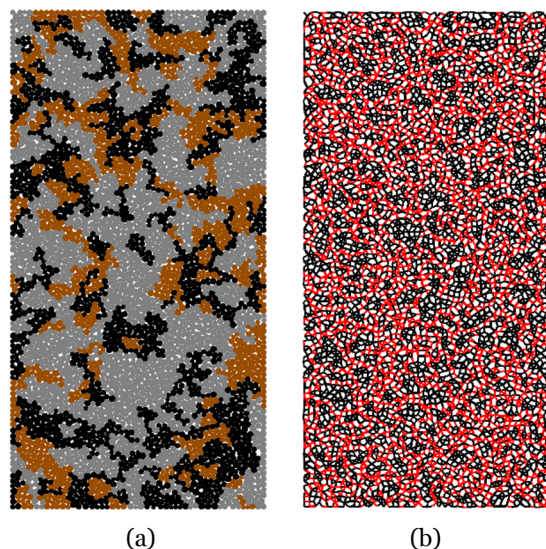


Fig. 3 Model establishment of rock samples: (a) Mineral distribution of rock samples; and (b) Distribution of the two types of contacts (the red item is intergranular contact, and the black one is the intragranular one)

Table 2 Micro-properties of particles and contacts for the established numerical model

Component	Quartz	Feldspar	Clay
General component			
Volume composite, V_{ratio} (%)	50	35	15
Particle			
Minimum ball radius, r_{min} (mm)	0.2		
Maximum/Minimum, r_{max}/r_{min}	1.66		
Ball density (kg/m ³)	2650	2600	2600
Intragranular contacts			
Stiffness ratio	1.9	2.4	1.8
Effective moduli (GPa)	210	103	40.2
Bond tensile strength, σ_b (MPa)	60	32	6.7
Bond cohesion, C_b (MPa)	200	95	40.2
Friction coefficient	0.5	0.5	0.5
Intergranular contacts			
Stiffness ratio	2.1		
Effective moduli (GPa)	110		
Bond tensile strength, σ_b (MPa)	50		
Bond cohesion, C_b (MPa)	100		
Friction coefficient	0.5		

Note: The intragranular contacts represent those inside one mineral grain, and the intergranular contacts represent those between two mineral grains.

In the experiments, the softening factors of four groups of sandstone specimens are η (0.5%) = 0.945, η (2%) = 0.580, η (3.5%) = 0.499, and η (5%) = 0.439, respectively. In the simulation, to simulate the weakening effect of rock with the increase of water content, the softening factors are calibrated to be 1.48, 3.3, 4.1, and 5.07, respectively. The uniaxial compression stress-strain curves in the experiments

and simulations are shown in Fig. 5. With the increase of water content, the slope of stress-strain curves becomes modest, and the uniaxial compression strength (UCS) reduces. In addition, the softening behavior after peak stress becomes clear. The macro-properties and failure characteristics of calibrated numerical models show a reasonable agreement with the laboratory tests, and the mechanical properties of

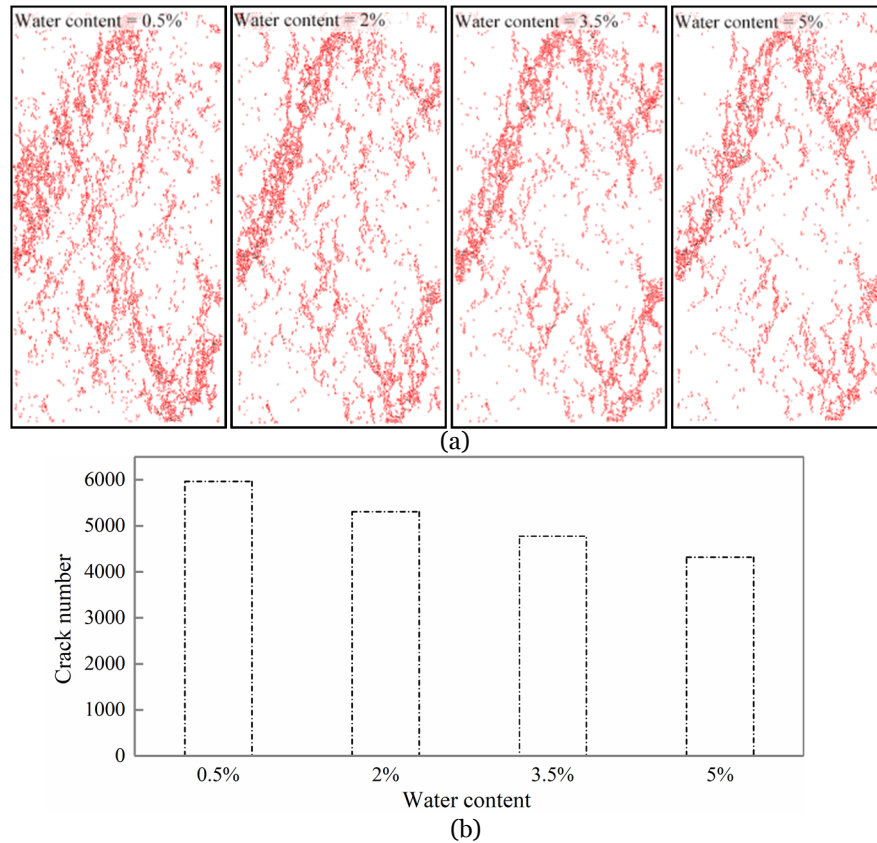


Fig. 4 Microcrack characteristics of numerical rock samples with different water contents under uniaxial compression tests. (a) Microcrack distribution under four water contents; (b) Microcrack number.

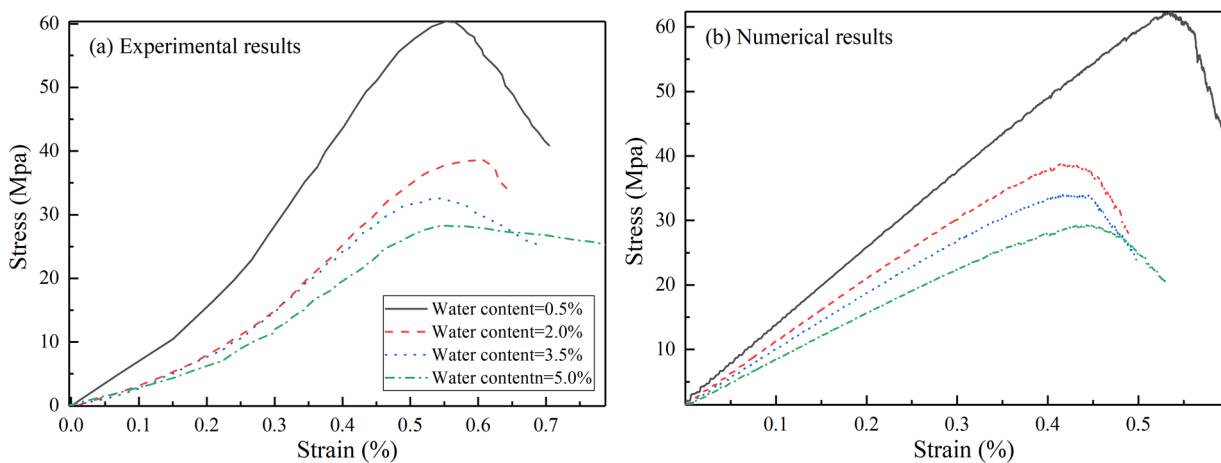


Fig. 5 Full stress-strain curves of rock samples with different water contents.

rock samples in the experiment and numerical simulation are basically similar (Table 3), further verifying the reliability of the numerical model.

Acoustic emissions (AE) are generated spontaneously during the rock failure process due to microcracking initiation. In the present simulation, the AE counts were obtained by counting the generated crack number in each 50 timesteps, as the rupture of every bond is assumed to be the source of an acoustic event since the failed bond results in the release of elastic energy stored in the elements (Li et al. 2016). According to the numerical simulation results (Fig.6), with the increase of water content, the peak of the AE event number shows a weakening trend, and the significant initiation of the acoustic emission signal starts early. This can be attributed to the increase of water content leading to the strength reduction of mineral particles that are easy to soften when encountering water. The cracks will be generated when the axial stress is small, and the acoustic emission intensity is further weakened when the peak strength is reached.

4 Results and Discussion

4.1 Effect of cyclic loading parameters on water-bearing sandstone

In reservoir engineering, rock mass is subjected to the cyclic impact of water flow due to its rise and fall. The storage volume of a reservoir corresponds to the maximum cyclic loading during cyclic loading. The water storage/drainage velocity corresponds to the loading frequency during cyclic loading, and the

Table 3 Physical mechanical property of rock in experimental and numerical results

Method	Parameter	Water content			
		0.5%	2%	3.5%	5%
Experiment results	Young's modulus E (GPa)	125.922	92.964	84.854	75.968
	Poisson's ratio ν	0.157	0.338	0.395	0.439
	UCS (MPa)	61.334	37.657	34.422	28.518
Numerical results	Young's modulus E (GPa)	116.85	87.81	76.45	64.09
	Poisson's ratio ν	0.152	0.343	0.39	0.416
	UCS (MPa)	62.397	38.805	33.956	29.364

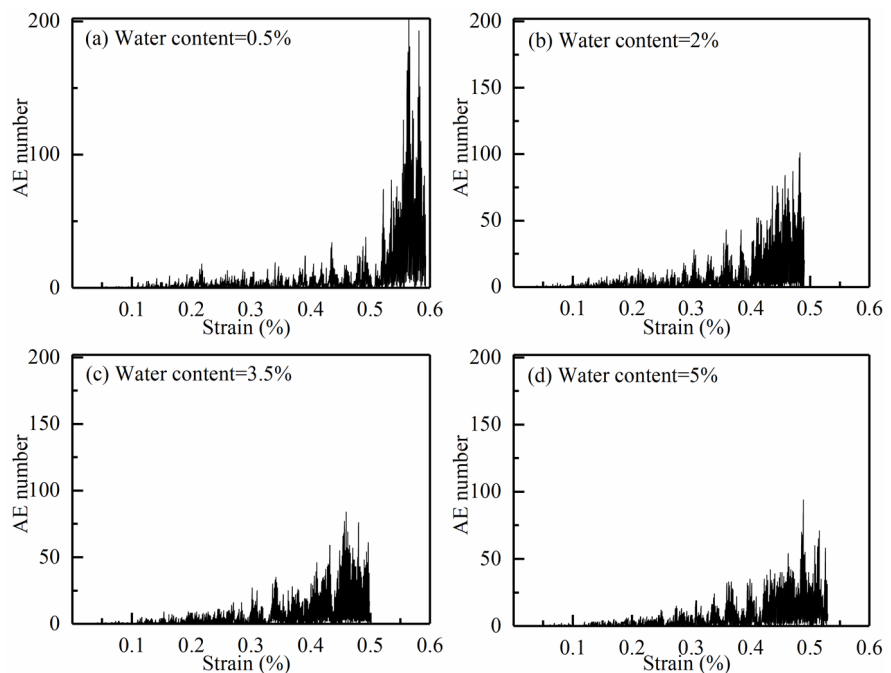


Fig. 6 Acoustic emissions (AE) count of rock samples with different water contents.

water storage/drainage difference corresponds to the loading amplitude during cyclic loading. The maximum cyclic loading, loading amplitude, and loading frequency will affect the fatigue mechanical properties of rock mass. Thus, studying the effect of various parameters on the mechanical properties of rock mass is useful for monitoring and evaluating reservoir stability. When the water content is 5%, the strength of most vulnerable rock samples is the lowest, so that 12 cyclic tests with different combinations of loading parameters were carried out on these high water-content samples (Table 4). What should be noted is that the parameter value of the simulation arrangements is based on the previous researches, and more reasonable ones will be conducted in the subsequent work.

4.1.1 Effect of loading amplitude

The loading amplitude level (A) represents the ratio of loading amplitude to the maximum loading

stress. In Fig. 7, it was found that during cyclic loading, the plastic strains will be gradually accumulated with the increase of cycle numbers until the samples are finally destroyed. The reason for generating the hysteresis loop is that during loading, rock mineral crystals appear on the friction slip, damage cracks emerge, and the rock deformation

includes elastic and plastic deformations. During the unloading stage, although the elastic deformation can be recovered, the irreversible strain caused by plastic deformation still exists.

To describe the damage of rocks under cyclic loading, in addition to irreversible strain, the damage variable E_d is introduced in this study, which can be defined as follows:

$$E_d = \frac{\varepsilon_{r(p)}}{\varepsilon_{r(f)}} \quad (3)$$

where $\varepsilon_{r(p)}$ is the irreversible strain and $\varepsilon_{r(f)}$ is the final irreversible strain.

In Fig. 8, the maximum stress level (M) is set at 0.95, and the cyclic loading frequency (F) is set at 1 Hz. In Fig. 8a, the relationship between axial irreversible strain and relative cycle numbers are revealed. The relative cycle number is the ratio of the current cycle number to the total cycle number. Under cyclic loading, when the amplitude coefficients are 0.6 and 0.7, the irreversible strain can be divided into three stages, namely, the initial stage, uniform velocity stage, and acceleration stage. Owing to the existence of the initial weak planes or minerals, the damage first accumulates sharply, so did the irreversible strain in the first few loading cycles. Then,

Table 4 Loading parameter combinations in cyclic tests

Number	Parameter combination		
	Frequency (Hz)	Maximum stress level	Amplitude level
1	1	0.95	0.6
2	1	0.95	0.7
3	1	0.95	0.8
4	1	0.95	0.9
5	0.1	0.95	0.7
6	1	0.95	0.7
7	1.5	0.95	0.7
8	5	0.95	0.7
9	1	0.8	0.7
10	1	0.85	0.7
11	1	0.9	0.7
12	1	0.95	0.7

Note: Maximum stress level represents the ratio between the applied stress and rock strength. Amplitude level represents the ratio between the maximum and minimum applied stresses difference to the rock strength.

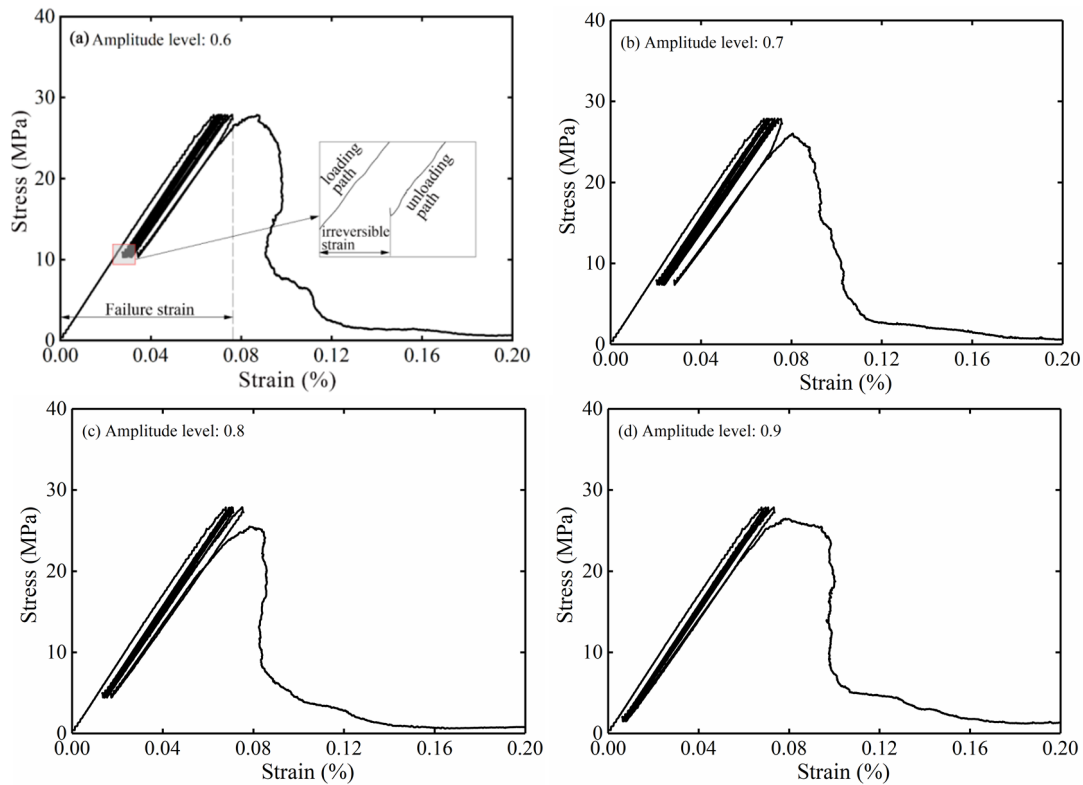


Fig. 7 Fatigue stress-strain curves under cyclic loading with different loading amplitude levels: frequency=1 Kz, maximum stress level=0.95.

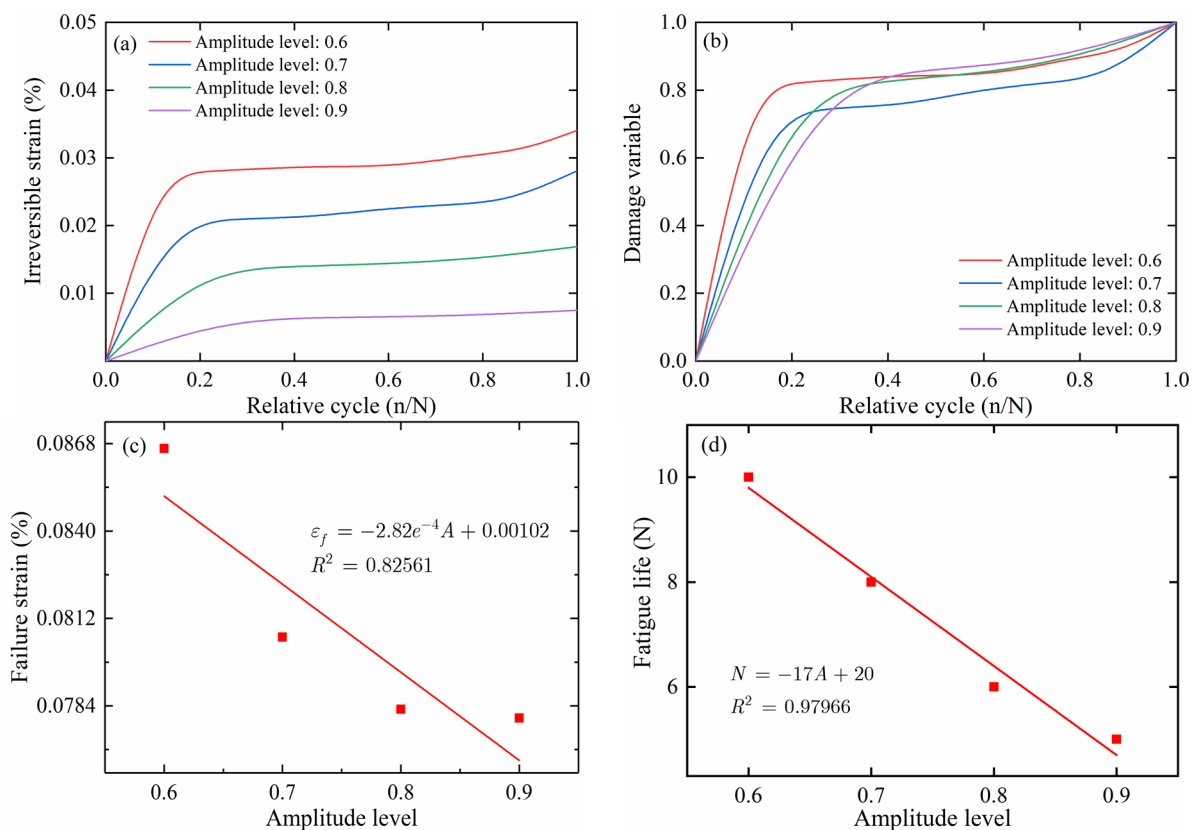


Fig. 8 Effect of loading amplitude level on fatigue properties of water-bearing sandstone: (a) Irreversible strain; (b) Damage variable; (c) Failure strain; (d) Fatigue life.

during the uniform speed phase, it increases slowly as the damage rate decreases. In the third stage, the irreversible strain increased rapidly again, resulting from the rapid crack propagation and coalescence, and finally leads to the macro-failure of rock sample. With the increase of amplitude level, the third stage becomes relatively less obvious, and the first and second stages dominate, which attributes to the fact that the higher stress amplitude will cause severer damage during the early loading stages. Meanwhile, the duration of the first phase also increased, and the final irreversible strain of rock decreased gradually.

The damage evolution is shown in Fig. 8b, the trend of which is similar to that of the irreversible strain. However, compared with the irreversible strain, the damage variable increases more obviously in the initial stage, indicating that the generated damage in the initial stage has a high proportion of overall damage. With the increase of amplitude level, the proportion of damage caused in the initial stage changes slightly which may attribute to the sample discreteness. The proportion of damage caused in the second stage remained relatively stable; the

proportion of damage caused in the third stage showed a slightly increasing trend. Overall, the amplitude level slightly affected the damage in the second and third stages.

Fig. 8c shows the effect of cyclic loading amplitude on the failure strain (i.e., the strain which represents that the rock will fail after a short period of time and can be seen as the failure indication, shown in Fig. 7a), which is significant for predicting the final failure of rock sample. When the amplitude level increased from 0.6 to 0.9, the failure strain shows a decreasing trend. Specifically, the failure strain almost decreases linearly from 0.0852% to 0.784%.

Fig. 8d shows the effect of loading amplitude on the fatigue life (loading number before rock failure). With the increase of amplitude, the fatigue life decreases linearly by 30% from the amplitude level of 0.9 to 0.6. On the whole, the influence of loading amplitude on fatigue life of water-bearing sandstone is not significant as the decreased cycle number is only 3.

Overall, with the increase of amplitude, because the maximum loading stress is fixed, the time of rock

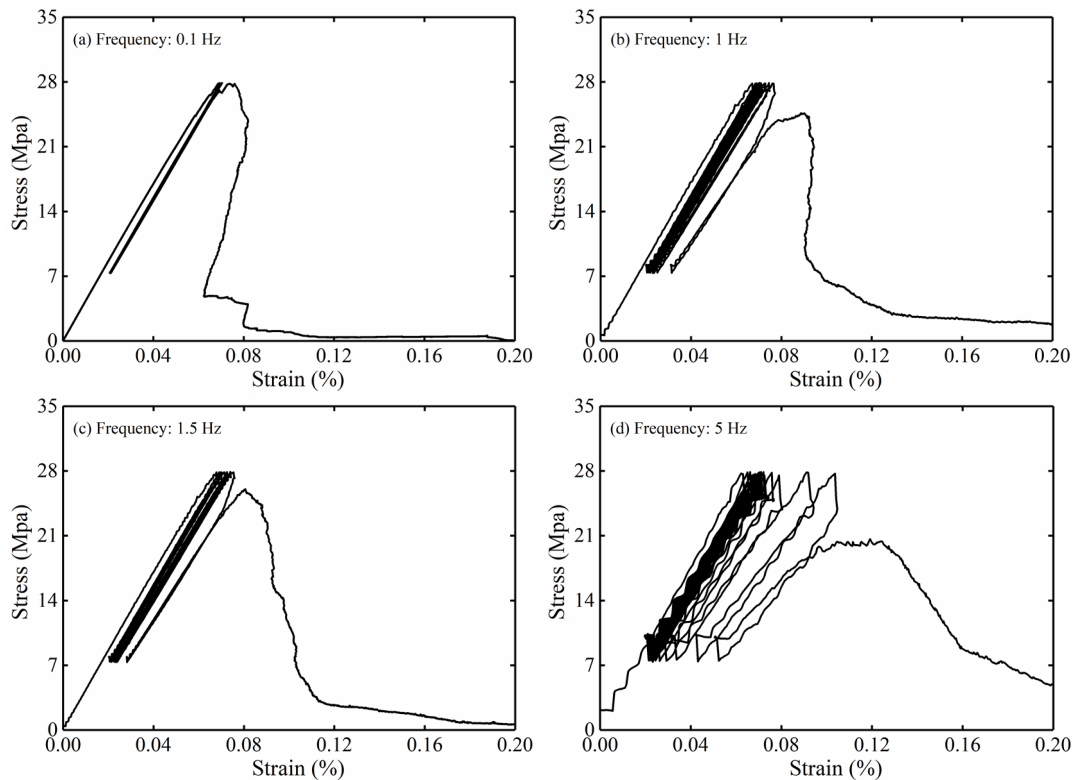


Fig. 9 Fatigue stress–strain curves under cyclic loading with different loading frequencies: amplitude level=0.7, maximum stress level=0.95.

at a high-stress level is relatively reduced. Therefore, the final irreversible strain of rock decreased with the increase of amplitude. Moreover, an increase of the amplitude has a limited effect on reducing the fatigue life of rock, and what should be also noted is that with the increase of loading amplitude, the irreversible deformation generated in the third stage is decreased, which means that under a large loading amplitude, it is not exact to predict the failure symptom of rock through the deformation.

4.1.2 Effect of loading frequency

When the amplitude level and maximum loading stress level are the same, Fig. 9 shows the stress-strain curves of water-bearing sandstone at different loading frequencies (0.1, 1, 1.5, and 5 Hz). It can be found that, under an ultralow frequency of 0.1 Hz, macro failure of rock occurs within a relatively short period of time, as the weak planes or minerals have enough time to break. While for the other cases, more time is needed for the final failure. In addition, with the increase of frequency, the hysteresis loops become sparser.

In Fig. 10a, for the loading frequency of 1 Hz, 1.5 Hz, and 5 Hz, the irreversible deformation shows an

obvious three-stage regulation, and with the increase of frequency, the third stage becomes more obvious, because the damage generates in the previous stages become slight. In the initial stage, the irreversible deformation increased rapidly in several cycles, and the proportion of irreversible deformation generated in the initial stage decreased with the increase of frequency, which attributes to the fact that the higher frequency, the effective loading time is shorter for the damage initiation. In the uniform velocity stage, the irreversible deformation accumulates slowly, taking the longest time. However, for the specimen with a loading frequency of 0.1 Hz, the irreversible deformation showed a two-stage development regulation, as the time for the former two stages is enough for the final failure. In addition, with the increase of loading frequency from 1 Hz to 5 Hz, the final irreversible strain also increases, but the final irreversible strain at 0.1 Hz is still the largest.

The damage evolution affected by the loading frequency is shown in Fig. 10b. The evolution characteristic of damage variable is almost consistent with the irreversible strain, i.e., for the loading frequency of 1 Hz, 1.5 Hz, and 5 Hz, an obvious three stage characteristic was observed during loading. In

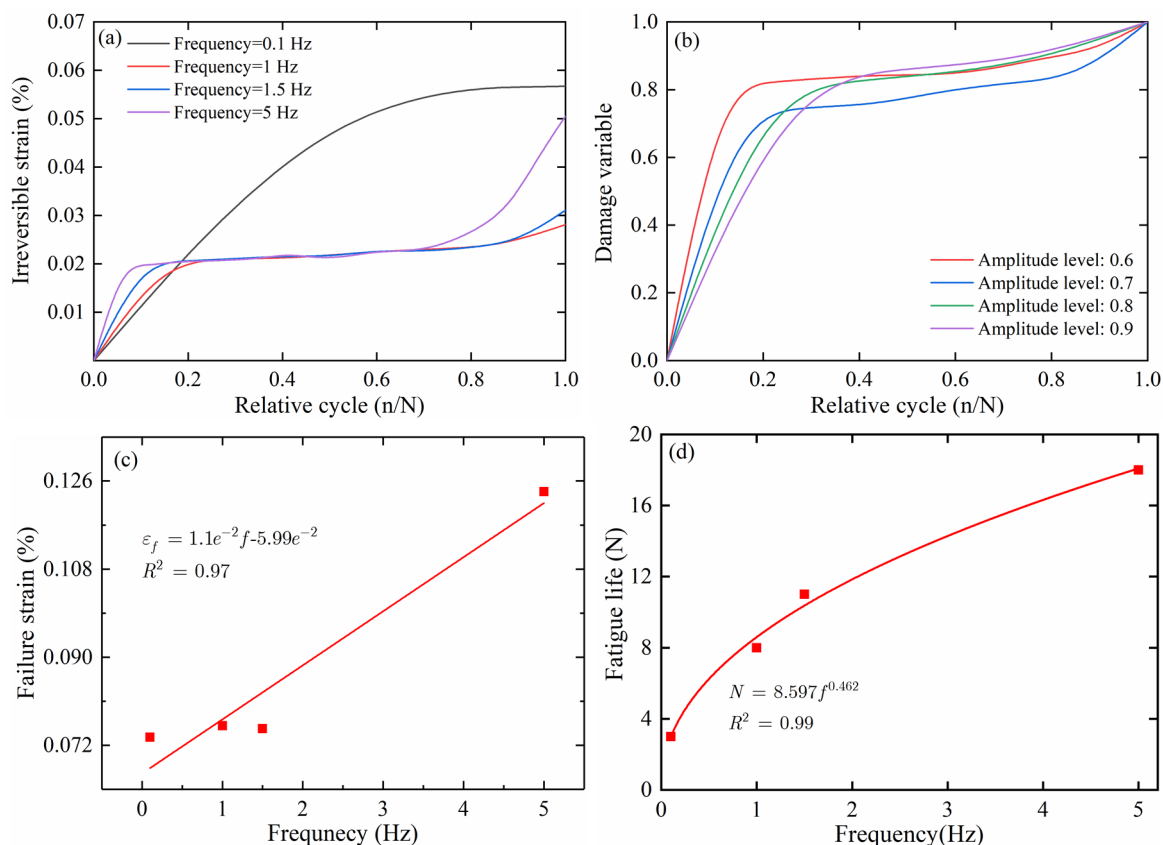


Fig. 10 Effect of loading frequency on fatigue properties of water-bearing sandstone: (a) Irreversible strain; (b) Damage variable; (c) Failure strain; (d) Fatigue life.

the first few cycles, the higher the loading frequency, the smaller the increase of damage variable. In the uniform velocity stage, the damage variable increased slowly, and no obvious difference was observed in the growth rate of damage variable under three frequencies. However, the higher the frequency, the faster it will reach the third stage. The loading frequency of 0.1 Hz showed a two-stage characteristic, especially the proportion of damage generated in the first stage is larger compared with the irreversible strain curve. This indicates that the damage generated in the initial loading is quite large when the frequency is low.

The relationship between the failure strain and loading frequency is shown in Fig. 10c. The failure strain is approximately increasing linearly with the loading frequency. When the loading frequency increases from 0.1 Hz to 5 Hz, the failure strain increases from 0.0736% to 0.124%.

Fig. 10d shows the effect of the loading frequency to the fatigue life. The loading number before rock failure increases exponentially with the increase of frequency: with the increase of loading frequency from 0.1 Hz to 5 Hz, the fatigue life of sample

increases from 3 cycles to 18 cycles. Thus, regarding the failure life, the effect of the loading frequency is greater than the amplitude level.

Overall, the difference in the fatigue characteristic of rock sample under different frequency cyclic loadings is caused by time effect. When the frequency is high, microcracks do not have enough time to propagate and intersect. Therefore, more cyclic loading numbers are needed for the rock to damage.

4.1.3 Effect of maximum loading stress

To further analyze the effect of maximum stress level of cyclic loading on the fatigue characteristics of water-bearing sandstone, four numerical tests were carried out. During the simulation, the loading frequency is 1 Hz, and the amplitude level is 0.7. The M was set to 0.8, 0.85, 0.9, and 0.95. The stress-strain curves for them are shown in Fig. 11. The differences between these curves are not significant, and all the hysteresis loops are relatively dense.

To obtain the damage evolution of rock under cyclic loading, the irreversible strain was counted, as shown in Fig. 12a. For different maximum stress

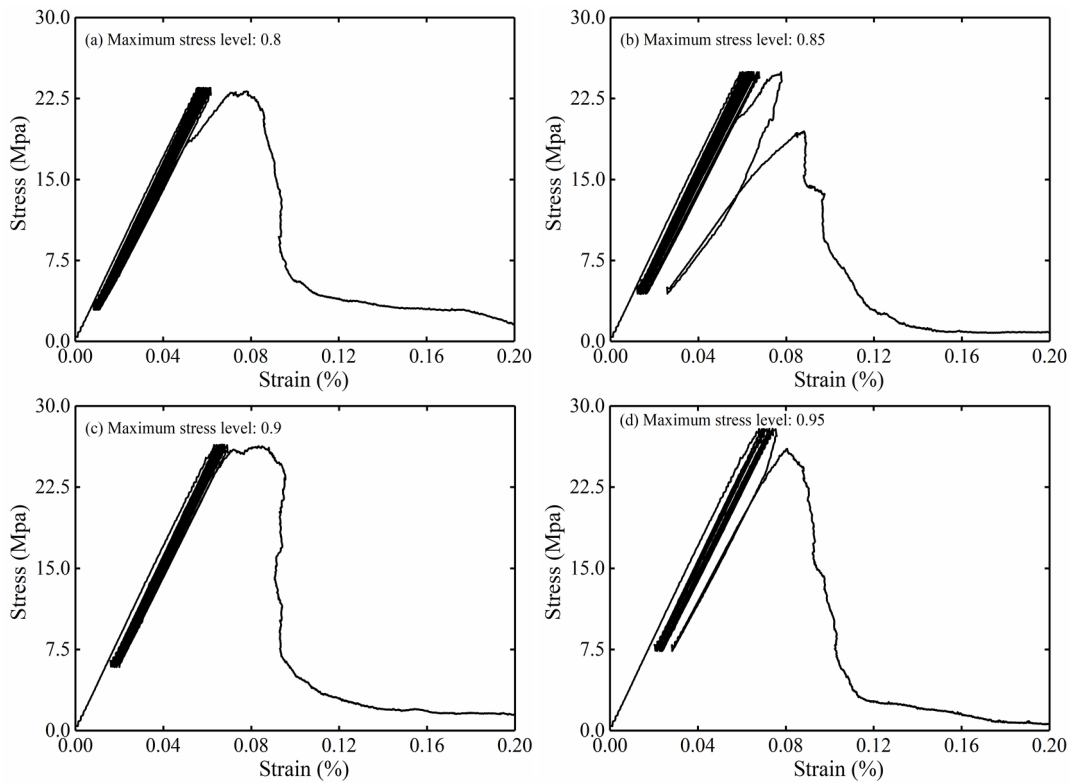


Fig. 11 Fatigue stress–strain curves under cyclic loading with different maximum stress levels: amplitude level=0.7, frequency=1 Hz.

levels, the curves of irreversible strain in respect of the relative cycle number showed three-stage characteristics. In the first stage, the deformation increases rapidly, and the increase range mainly depends on the maximum loading stress. With the increase of the maximum loading stress, the increased magnitude of the first stage grows, and the duration time of first stage also increases, because it is easier to generate initial damage.

The damage evolution under four working conditions is shown in Fig. 12b. In the initial stage, significant damage will be accumulated in several cycles. Especially for the maximum loading stress of 0.8, the damage variable in the initial stage increases almost vertically attribute to the smaller amount of initial damage that can generate. With the increase of the maximum loading stress, the increasing trend slowed down. This indicates that the lower the maximum loading stress, the larger the proportion of damage in the initial stage, and the smaller the growth rate of damage in the latter cyclic loading.

The evolution of the failure strain in respect of the maximum loading stress is shown in Fig. 12c. The failure strain is linearly proportional to the maximum loading stress. With the maximum loading stress

varying from 0.8 to 0.95, the failure strain increases from 0.0614% to 0.0754%.

Fig. 12d shows the relationship between cyclic loading number and maximum loading stress. The cyclic loading number shows an exponential relationship with the maximum loading stress, similar to the relationship between cyclic loading number and loading frequency, but the impact degree is greater. As the maximum loading stress increases from 0.8 to 0.95, the fatigue life decreases from 114 cycles to 8 cycles.

It can be found from Table 5 that both the relationships between maximum stress, failure strain, and fatigue life of the present simulation generally obey that obtained from experiments (Geranmayeh-Vaneghi et al. 2020). The difference between them should be attributed to two reasons: the first one is the variation between samples; the second one is the loading frequency (i.e., the numerical one is 1 Hz, while the experimental one is 0.1 Hz), as higher the loading frequency, longer the fatigue life and lower the failure strain.

With the increase of maximum loading stress, the average stress applied to rock sample increases. Therefore, it is easier to reach the strength limit of mutually bonded mineral particles, i.e., it is easier to produce damage, and the fatigue life is shorter.

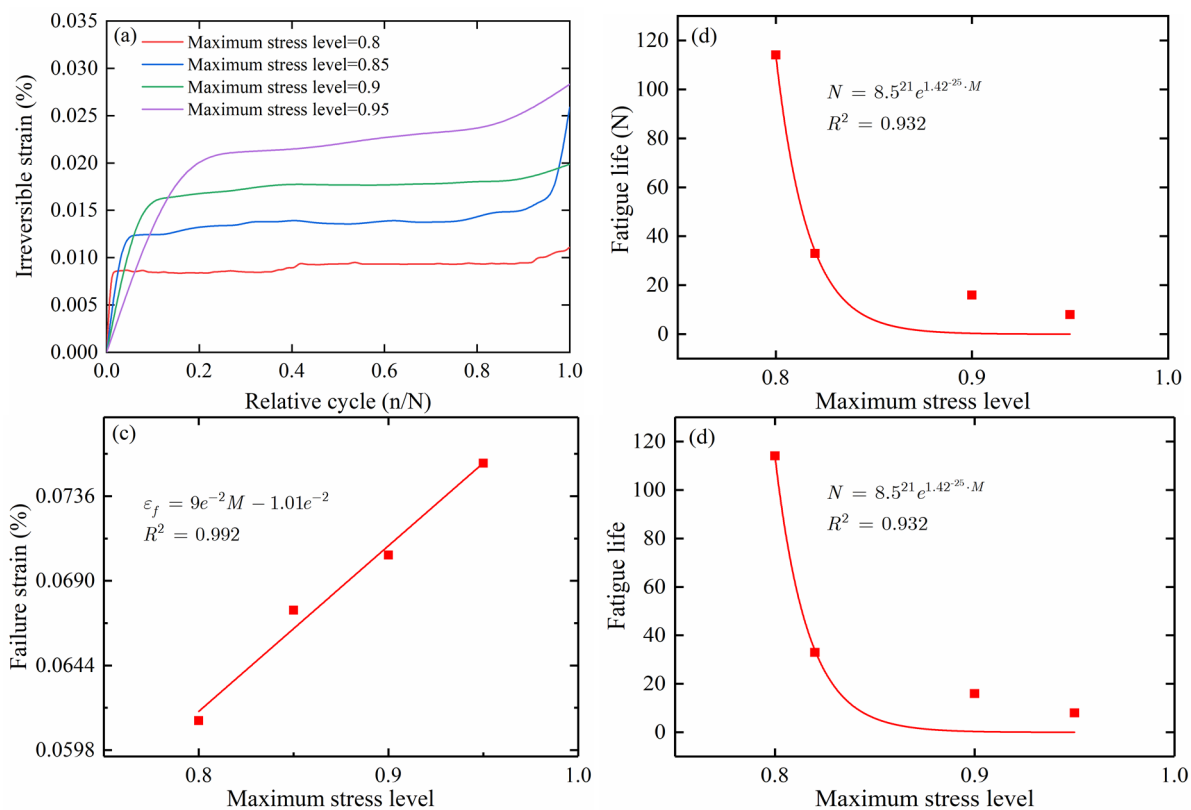


Fig. 12 Effect of maximum loading stress on fatigue properties of water-bearing sandstone: (a) Irreversible strain; (b) Damage variable; (c) Failure strain; (d) Fatigue life.

Table 5 The comparison of the fitting equation for the maximum stress, failure strain, and fatigue life between simulations and experiments (Geranmayeh-Vaneghi et al. 2020)

Parameters	Numerical	Experimental
Failure strain	$\epsilon_f = 9e^{-2}M - 1.01e^{-2}$	$\epsilon_f = 2.45e^{-3}M + 4.36e^{-2}$
Fatigue life	$N = 8.5^{21}e^{1.42^{-25}M}$	$N = 2^{11}e^{-0.239M}$

Note: ϵ_f is the failure strain, M is the maximum stress level, and N is the fatigue life.

Moreover, due to the fixed lower stress, an increase of the maximum loading stress also increases the duration time for rock suffering high stress, leading to more irreversible deformation.

Overall, considering the fatigue life, which is the most important factor, for the water-bearing sandstone, the loading amplitude has the least effect on the fatigue characteristics, followed by the loading frequency, and the maximum loading stress has the largest effect. Thus, the conditions when the highest water store level continuously increases and reaches a warning level, it should be paid more attention to monitor the safety and stability of the reservoirs. In addition, the failure strain for the water-bearing sandstone is in the range of around 0.0614% to 0.126%, which is meaningful for predicting.

4.2 Effect of water content on water-bearing sandstone

In the present study, the uniaxial cyclic loading tests were also conducted on the samples with different water contents. The loading parameters performed are: loading frequency is 1 Hz, amplitude level is 0.7, and the maximum stress level is 0.95. The obtained stress-strain curves are depicted in Fig. 13. It can be easily found that, besides the maximum stress, there is no obvious difference. In addition, all the hysteresis of the obtained stress-strain curves shows similar characteristics with small numbers of dense loops.

As shown in Fig. 14(a, b), both the irreversible deformation and damage evolution can be divided into two stages, and the generated residual strain and damage in the initial stage dominate. In the first stage,

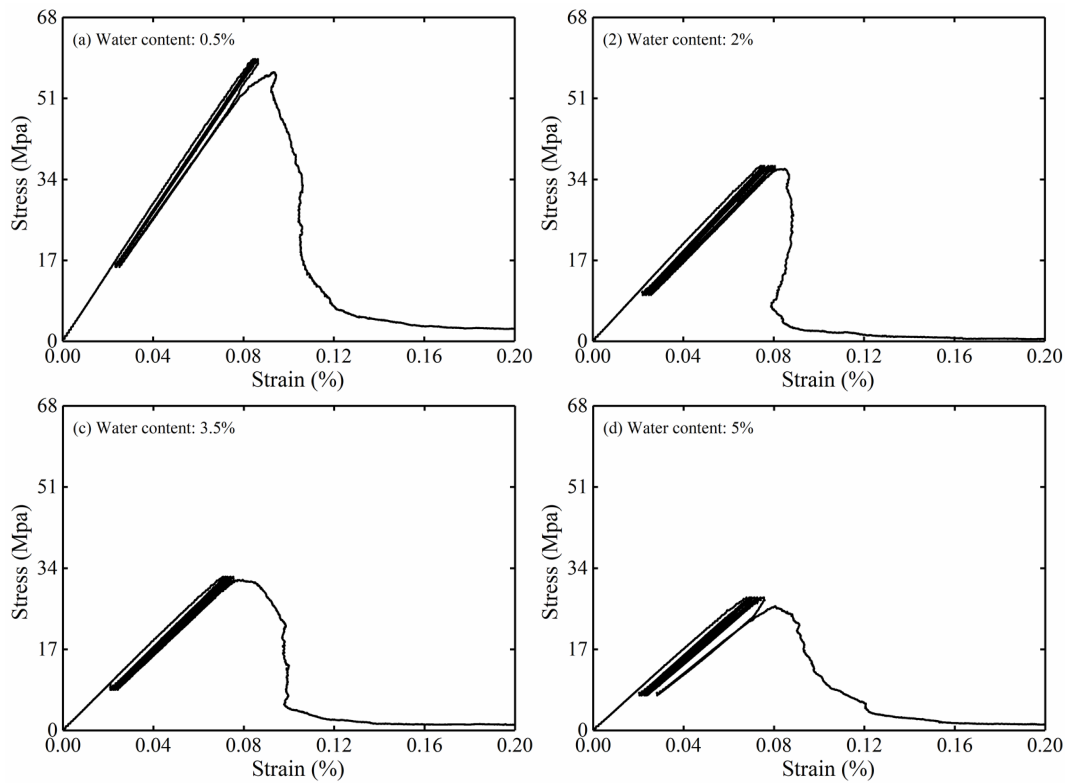


Fig. 13 Fatigue stress–strain curves of samples with different water contents under cyclic loading: amplitude level=0.7, frequency=1 Hz, maximum stress level=0.95.

the irreversible deformation and damage increases rapidly in the initial cycles, and then approaching the uniform velocity stage, when the irreversible deformation and damage accumulate slowly. Similar to the stress-strain curves, the water content makes a little difference, which indicated that the water content plays a slight influence on the fatigue behavior of water-bearing sandstone.

The relationship between the failure strain and water content is shown in Fig. 14c. The failure strain approximately decreases linearly with the water content, however, the increasing magnitude is not significant: when the water content increases from 0.5% to 5%, the failure strain increases from 0.0864% to 0.07558%.

Fig. 14d illustrates the effect of the water content on the fatigue life. Generally speaking, the cyclic loading number increases linearly with the water content, which attributes to the fact that the ductility of sandstone increases with the water content. However, what should be noted is that, although the maximum stress level is the same, the maximum stress is significantly different from each other. It is easy to accept that when applying higher maximum stress to the samples with high water contents, the

fatigue life will decrease accordingly.

4.3 Fracture process of water-bearing sandstone

For the above 16 working conditions, there are mainly two types of failure modes as shown in Fig. 15 (blocks with different colors represent fragments). When the water content is low (i.e., $w=0.5\%$), the fatigue failure mode is tensile splitting failure (Fig. 15b), indicating that the water content significantly affects the failure mechanism of water-bearing sandstone. For the higher water content (i.e., $w=2, 3.5, 5\%$), the samples exhibit shear failure characteristic: an inverted V-shaped macrocrack occurs in the rock. Compared with the static compression test simulation (Fig. 15a), the integrity of rock fragments under cyclic loading is poor, and more powder fragments are produced, one of the typical characteristics of rock fatigue damage (Liu et al. 2021). In addition, it was found that the loading parameters almost have no effect on the failure mode.

Fig. 16 shows the AE characteristics of water-bearing sandstone under cyclic loading with a frequency of 1 Hz, loading amplitude level of 0.9, and

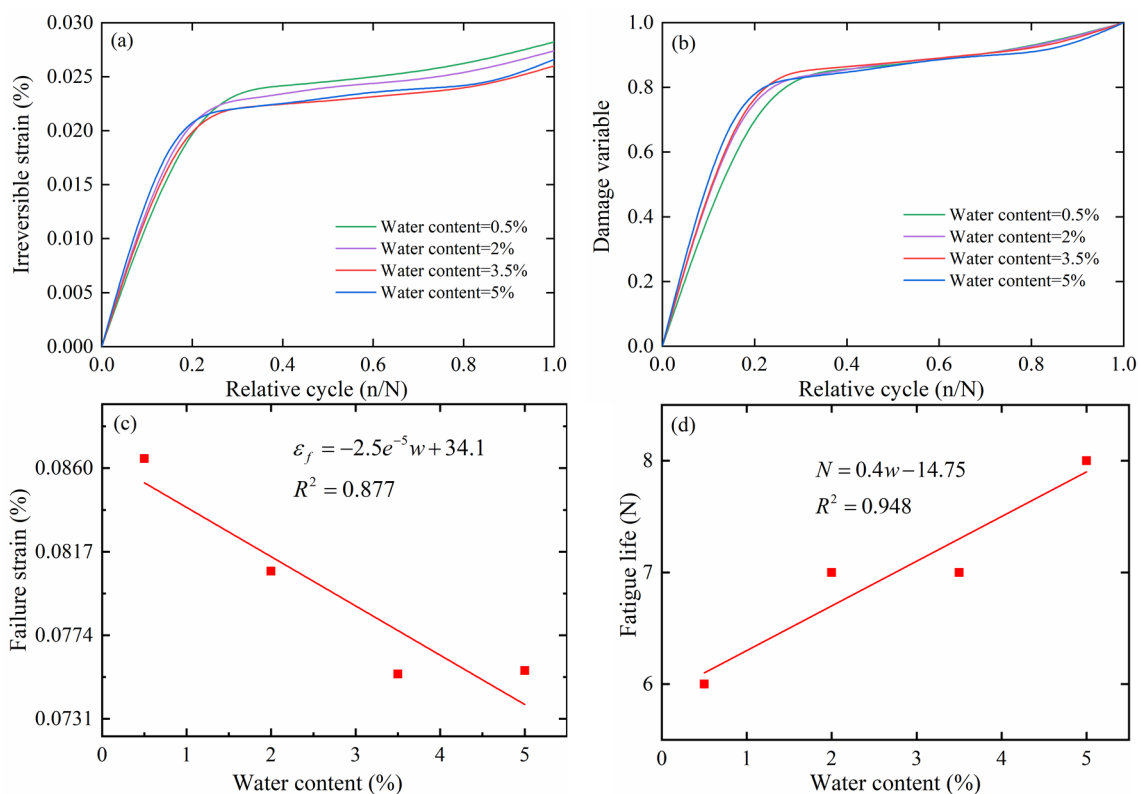


Fig. 14 Effect of water content on fatigue properties of water-bearing sandstone: (a) Irreversible strain; (b) Damage variable; (c) Failure strain; (d) Fatigue life.

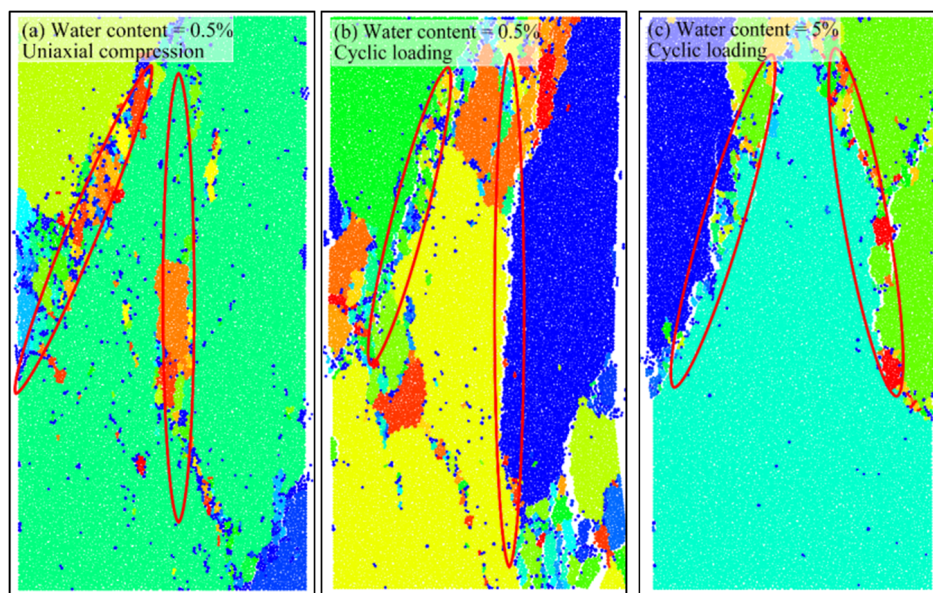


Fig. 15 Typical failure modes of numerical water-bearing sandstone model under uniaxial and cyclic loading conditions: (a) water content of 0.5% under uniaxial compression; (b) water content of 0.5% under cyclic loading compression; (c) water content of 5% under cyclic loading.

maximum loading stress of 0.95. Both the AE counts in the initial loading stage and the final failure stage is significant. In addition, compared with the initial stage, the acoustic emission intensity and energy

release of the final failure stage are higher, while they are gentle and uniform in the second stage. The initial damage results from the failure of the original weak planes, and thus, there is no significant AE count in

the second stage. At the final failure stage, with the generation of cracks, the stress concentration of the specimen becomes more intensified, and causing the rapid increase of AE counts. Therefore, AE technology is an effective method for monitoring the stability of dam and reservoir rock mass. By analyzing the AE signature obtained from the sensors buried inside the warning rock of the reservoirs, the real-time condition of it can be readily captured and further treatment can be designed based on this.

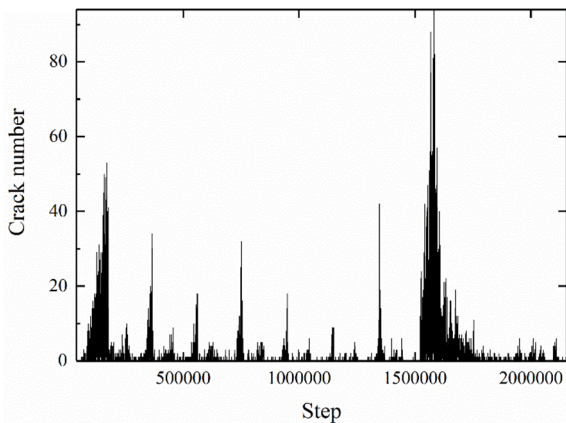


Fig. 16 Acoustic emissions (AE) count of rock samples during cyclic loading with a frequency of 1 Hz, loading amplitude level of 0.9, and maximum stress level of 0.95.

Fig. 17 shows the evolution regulation of crack numbers of water-bearing sandstone under cyclic loading with different amplitude, frequency, and maximum stress levels. Similar to the evolution regulation of irreversible strain, the number of cracks also showed the three-stage evolution characteristics. During the cyclic loading process, with the stress level exceeding the bond strength between particles, the cracks first increased uniformly and rapidly in the first few loading cycles. In the second stage, the number of cracks increases slowly in a step-by-step manner and then increases sharply again. Finally, macro failure of rock occurs. After the rock failure, the number of broken bonds is almost constant. Moreover, for different loading amplitudes, the difference in final crack number between them is small. For different frequencies, except for the loading frequency of 0.1 Hz (which can be seen as under the static condition), the other curves basically show a similar trend. For different maximum loading stress values, the evolution characteristics and crack numbers in the first and second stages under four loading conditions are basically the same. However, with the increase of maximum loading stress, the

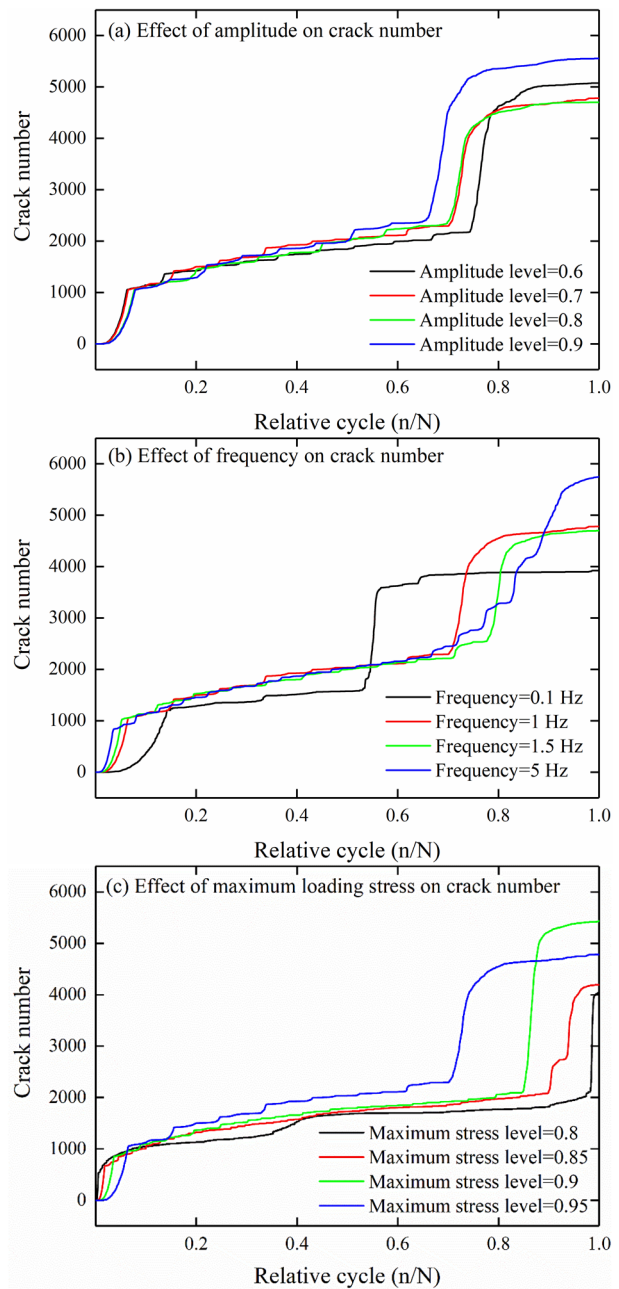


Fig. 17 Cracking evolution of water-bearing sandstone under cyclic loading with different amplitudes levels, frequencies, and maximum stress levels.

third stage appears earlier. This is consistent with the effect of various parameters previously analyzed on rock fatigue characteristics.

5 Conclusion

In this study, the water-bearing sandstone samples were established using the novel soft-bond contact model based on PFC2D. The effect of water

content and cyclic loading parameters related to the storage condition of reservoir on the deformability and damage evolution behavior of sandstone was evaluated. From the experimental and numerical results, the following conclusions are drawn.

(1) The mineral particles show obvious argillization phenomenon with a higher water content, and a large number of flaky structures appear. The smoother surface leads to the degradation of the macroscopic mechanical properties.

(2) The maximum stress is the parameter that mostly influences the fatigue life of the water-bearing sandstone, followed by the frequency, and then the loading amplitude. With the increase of loading amplitude, the relative duration of rock suffering with high stress is reduced, causing the decrease of the final irreversible strain. For the loading frequency, its effect on fatigue characteristics can be attributed to the time effect. When the frequency is high, microcracks do not have enough time to propagate and intersect, and more cyclic loading is needed for failure. With the increase of maximum stress, the average stress applied and the duration of rock suffering from high stress increase. Therefore, it is easier to reach the strength limit, and the fatigue life is shorter. For the water content, it exhibits a slight influence on the damage evolution of sandstone under the same cyclic loading conditions.

(3) There are mainly two kinds of failure modes for the used water-bearing sandstone under cyclic loading conditions: tensile splitting failure and shear failure. The failure mode is almost unaffected by the loading parameters, while the effect of the water content is enormous. The AE counts in the initial

loading stage and final failure stage are significant. The reason for the former one is the damage of the initial weak planes, for the latter one, the rapid generation and propagation of cracks. Therefore, AE is an effective method for monitoring the stability of the reservoir engineering.

The used sandstone in the present work is relatively homogeneous, which leads to the uniform failure mode (e.g., splitting failure). However, there are numerous kinds of natural sandstone with different mineralogical characteristics (e.g., grain fabric, mineral compositions), which pose a great effect on the failure mode. Thus, the subsequent researches will mainly focus on comparing the differences in the mechanical behaviors of sandstones based on the experiments and simulations. In addition, the numerical model to reproduce the mechanical behavior sandstone will be further updated (e.g., simulate the expansion behavior of water-sensitive minerals after absorbing water).

Acknowledgments

This work was supported by the National Natural Science Foundation of China (No. 52104125), the funding of State Key Laboratory for GeoMechanics and Deep Underground Engineering, China University of Mining & Technology, Beijing (SKLGDUEK2133), the funding of Key Laboratory of Rock Mechanics and Geohazards of Zhejiang Province (No. ZJRMG-2020-02), and the Fundamental Research Funds for the Central Universities.

References

- Azhar M, Zhou H, Yang F, et al. (2020) Water-induced softening behavior of clay-rich sandstone in Lanzhou Water Supply Project, China. *J Rock Mech Geotech* 12: 557-570. <https://doi.org/10.1016/j.jrmge.2019.07.017>
- Bagde M N, Petroš V (2005) Fatigue properties of intact sandstone samples subjected to dynamic uniaxial cyclical loading. *Int J Rock Mech Min* 42(2): 237-250. <https://doi.org/10.1016/j.ijrmmms.2004.08.008>
- Chen Y, Zhang Y, Li X (2019) Experimental study on influence of bedding angle on gas permeability in coal. *J Petrol Sci Eng* 179: 173-179. <https://doi.org/10.1016/j.petrol.2019.04.010>
- Feng G, Wang X, Kang Y, et al. (2020) Effect of thermal cycling-dependent cracks on physical and mechanical properties of granite for enhanced geothermal system. *Int J Rock Mech Min* 134: 104476. <https://doi.org/10.1016/j.ijrmmms.2020.104476>
- Feng G, Wang X, Wang M, et al. (2020) Experimental investigation of thermal cycling effect on fracture characteristics of granite in a geothermal-energy reservoir. *Eng Fract Mech* 235: 107180. <https://doi.org/10.1016/j.engfracmech.2020.107180>
- Feng W, Qiao C, Niu S, et al. (2019) Macro-mechanical properties of saturated sandstone of Jushan Mine under post-peak cyclic loading: an experimental study. *Arab J Geosci* 12(23): 702. <https://doi.org/10.1007/s12517-019-4904-0>
- Geranmayeh-Vaneghi R, Ferdosi B, Okoth AD, et al. (2018) Strength degradation of sandstone and granodiorite under uniaxial cyclic loading. *J Rock Mech Geotech* 10(1): 117-126. <https://doi.org/10.1016/j.jrmge.2017.09.005>
- Geranmayeh-Vaneghi R, Thoeni K, Dyskin AV, et al. (2020) Fatigue damage response of typical crystalline and granular rocks to uniaxial cyclic compression. *Int J Fatigue* 138:

105667.
<https://doi.org/10.1016/j.ijfatigue.2020.105667>
- Ghazvinian E, Diederichs M S, Quey R (2014) 3D random Voronoi grain-based models for simulation of brittle rock damage and fabric-guided micro-fracturing. *J Rock Mech Geotech* 6(6): 506-521.
<https://doi.org/10.1016/j.jrmge.2014.09.001>
- Guo Y, Jiang X, Song Z (2018) Analysis of seepage evolution law of rock mass based on the numerical algorithm considering strength weakening water absorption. *Arab J Geosci* 11(13): 349.
<https://doi.org/10.1007/s12517-018-3630-3>
- Horn HM, Deere DU (1962) Frictional Characteristics of Minerals. *Géotechnique* 12(4): 319-335.
<https://doi.org/10.1680/geot.1962.12.4.319>
- Itasca (2018) PFC2D manual Version 6.0. ICG, Minneapolis, Minnesota.
- Li H, Zhong Z, Eshiet KI, et al. (2020) Experimental investigation of the permeability and mechanical behaviours of chemically corroded limestone under different unloading conditions. *Rock Mech Rock Eng* 53(4): 1587-1603.
<https://doi.org/10.1007/s00603-019-01961-y>
- Li H, Zhong Z, Liu X, et al. (2018) Micro-damage evolution and macro-mechanical property degradation of limestone due to chemical effects. *Int J Rock Mech Min* 110: 257-265.
<https://doi.org/10.1016/j.ijrmms.2018.07.011>
- Li K, Cheng Y, Fan X (2018) Roles of model size and particle size distribution on macro-mechanical properties of Lac du Bonnet granite using flat-joint model. *Comput Geotech* 103: 43-60.
<https://doi.org/10.1016/j.compgeo.2018.07.007>
- Li W, Wang X, Cheng J (2019) Measurement of the anisotropic elastic properties of shale: uncertainty analysis and water effect. *B Eng Geol Environ* 78(8): 6075-6087.
<https://doi.org/10.1007/s10064-019-01517-y>
- Li X F, Li H B, Liu Y Q, et al. (2016) Numerical simulation of rock fragmentation mechanisms subject to wedge penetration for TBMs. *Tunn Undergr Sp Tech* 53: 96-108.
<https://doi.org/10.1016/j.tust.2015.12.010>
- Li X, Peng K, Peng J, et al. (2021) Effect of cyclic wetting-drying treatment on strength and failure behavior of two quartz-rich sandstones under direct shear. *Rock Mech Rock Eng*.
<https://doi.org/10.1007/s00603-021-02583-z>
- Li X, Peng K, Peng J, et al. (2021) Experimental investigation of cyclic wetting-drying effect on mechanical behavior of a medium-grained sandstone. *Eng Geol* 293: 106335.
<https://doi.org/10.1016/j.enggeo.2021.106335>
- Liu E, He S (2012) Effects of cyclic dynamic loading on the mechanical properties of intact rock samples under confining pressure conditions. *Eng Geol* 125: 81-91.
<https://doi.org/10.1016/j.enggeo.2011.11.007>
- Liu Y, Dai F (2018) A damage constitutive model for intermittent jointed rocks under cyclic uniaxial compression. *Int J Rock Mech Min* 103: 289-301.
<https://doi.org/10.1016/j.ijrmms.2018.01.046>
- Liu Y, Dai F (2021) A review of experimental and theoretical research on the deformation and failure behavior of rocks subjected to cyclic loading. *J Rock Mech Geotech*.
<https://doi.org/10.1016/j.jrmge.2021.03.012>
- Liu Y, Dai F, Dong L et al. (2018) Experimental investigation on the fatigue mechanical properties of intermittently jointed rock models under cyclic uniaxial compression with different loading parameters. *Rock Mech Rock Eng* 51(1): 47-68.
<https://doi.org/10.1007/s00603-017-1327-7>
- Liu Y, Dai F, Feng P, et al. (2018) Mechanical behavior of intermittent jointed rocks under random cyclic compression with different loading parameters. *Soil Dyn Earthq Eng* 113: 12-24. <https://doi.org/10.1016/j.soildyn.2018.05.030>
- Liu Y, Dai F, Zhao T, et al. (2017) Numerical investigation of the dynamic properties of intermittent jointed rock models subjected to cyclic uniaxial compression. *Rock Mech Rock Eng* 50(1): 89-112.
<https://doi.org/10.1007/s00603-016-1085-y>
- Meng Q, Zhang M, Zhang Z, et al. (2018) Experimental research on rock energy evolution under uniaxial cyclic loading and unloading compression. *Geotech Test J* 41(4): 717-729.
<https://doi.org/10.1520/GTJ20170233>
- Morrow CA, Moore DE, Lockner DA (2000) The effect of mineral bond strength and adsorbed water on fault gouge frictional strength. *Geophys Res Lett* 27(6): 815-818.
<https://doi.org/10.1029/1999GL008401>
- Nguyen NHT, Bui HH, Kodikara J, et al. (2019) A discrete element modelling approach for fatigue damage growth in cemented materials. *Int J Plasticity* 112: 68-88.
<https://doi.org/10.1016/j.ijplas.2018.08.007>
- Niu S, Ge S, Yang D, et al. (2018) Mechanical properties and energy mechanism of saturated sandstones. *J Cent South Univ* 25(6): 1447-1463.
<https://doi.org/10.1007/s11771-018-3839-z>
- Peng K, Zhou J, Zou Q, et al. (2019) Deformation characteristics of sandstones during cyclic loading and unloading with varying lower limits of stress under different confining pressures. *Int J Fatigue* 127: 82-100.
<https://doi.org/10.1016/j.ijfatigue.2019.06.007>
- Qin Z, Fu H, Chen X (2019) A study on altered granite meso-damage mechanisms due to water invasion-water loss cycles. *Environ Earth Sci* 78(428).
<https://doi.org/10.1007/s12665-019-8426-6>
- Song Z, Konietzky H, Herbst M (2019) Three-dimensional particle model based numerical simulation on multi-level compressive cyclic loading of concrete. *Constr Build Mater* 225: 661-677.
<https://doi.org/10.1016/j.conbuildmat.2019.07.260>
- Tao Z, Chun Z, Yong W, et al. (2018) Research on stability of an open-pit mine dump with fiber optic monitoring. *Geofluids* 2018: 9631706.
<https://doi.org/10.1155/2018/9631706>
- Wang Q, He M, Li S, et al. (2021) Comparative study of model tests on automatically formed roadway and gob-side entry driving in deep coal mines. *Int J Min Sci Techno* 31(4): 591-601.
<https://doi.org/10.1016/j.ijmst.2021.04.004>
- Wang Z, Liu X, Zhong Z, et al. (2019) Mechanical response and energy dissipation mechanism of sandstone under cyclic dynamic loading using particle flow code simulations. *Ekoloji* 28(107): 4501-4512
- Xiao F, Jiang D, Wu F, et al. (2021) Deformation and failure characteristics of sandstone subjected to true-triaxial unloading: An experimental and numerical study. *Fatigue Fract Eng M* 44(7): 1862-1882.
<https://doi.org/10.1111/ffe.13470>
- Yang S, Yin P, Zhang Y, et al. (2019) Failure behavior and crack evolution mechanism of a non-persistent jointed rock mass containing a circular hole. *Int J Rock Mech Min* 114: 101-121.
<https://doi.org/10.1016/j.ijrmms.2018.12.017>
- Zhang X, Wong LNY (2014) Choosing a proper loading rate for bonded-particle model of intact rock. *Int J Fracture* 189(2): 163-179.
<https://doi.org/10.1007/s10704-014-9968-y>
- Zhao B, Liu D, Li Z, et al. (2018) Mechanical behavior of shale rock under uniaxial cyclic loading and unloading condition. *Adv Civ Eng* 2018: 9750480.
<https://doi.org/10.1155/2018/9750480>
- Zhu C, Zhang K, Cai H, et al. (2019) Combined Application of optical fibers and CRLD bolts to monitor deformation of a pit-in-pit foundation. *Adv Civ Eng* 2019: 2572034.
<https://doi.org/10.1155/2019/2572034>